Energy Transmission by Photon Tunneling in Multilayer Structures Including Negative Index Materials

C. J. Fu

Z. M. Zhang[1]
e-mail: zzhang@mail.me.gatech.edu

George W. Woodruff School
of Mechanical Engineering,
Georgia Institute of Technology, Atlanta, Georgia
30332, USA

D. B. Tanner
Department of Physics,
University of Florida, Gainesville, Florida 32611,
USA

The phenomenon of photon tunneling, which depends on evanescent waves for radiative transfer, has important applications in microscale energy conversion devices and near-field optical microscopy. In recent years, there has been a surge of interest in the so-called negative index materials (NIMs), which have simultaneously negative electric permittivity and negative magnetic permeability. The present work investigates photon tunneling in multilayer structures consisting of positive index materials (PIMs) and NIMs. Some features, such as the enhancement of radiative transfer by the excitation of surface polaritons for both polarizations, are observed in the predicted transmittance spectra. The influence of the number of layers on the transmittance is also examined. The results suggest that the enhanced tunneling transmittance by polaritons also depends on the NIM layer thickness and that subdividing the PIM/NIM layers to enhance polariton coupling can reduce the effect of material loss on the tunneling transmittance.
[DOI: 10.1115/1.2010495]

Keywords: Electromagnetic, Microscale, Properties, Radiation, Thin Films

1 Introduction

An evanescent wave is an electromagnetic field that decays exponentially in space and does not transfer energy. If two objects are separated by a very small distance (barrier), two evanescent waves that decay in opposite directions can interact with each other to produce a net energy flow through the barrier. This phenomenon, known as photon tunneling or radiation tunneling, is very important for radiative energy transfer between two bodies when the distance of separation is shorter than the dominant wavelength of the emitting source [1]. Cryogenic insulation is a practical example of when photon tunneling may be significant [2]. Advances in micro- and nanotechnologies have made it possible for radiative transfer by photon tunneling to be appreciable and even dominant at room temperature or above. Scanning near-field optical microscopy (SNOM) relies on the photon tunneling between the probe and the sample surface to provide images of the sample with a subwavelength spatial resolution [3,4]. The concept of microscale thermophotovoltaic devices utilizes photon tunneling to improve the efficiency, with the receiver placed in close proximity to the emitter [5]. Recent studies have shown that excitation of surface polaritons can greatly change the radiation spectrum so that nearly monochromatic emission occurs close to the surface of the emitter; consequently, both the net radiative energy flux and the energy conversion efficiency could increase tremendously at the microscale [6,7].

The concept of a negative refractive index ($n<0$) was first postulated by Veselago [8] for a hypothetical material that has both negative electric permittivity (ε) and negative magnetic permeability (μ) in the same frequency region. (Note that ε and μ in the present paper are relative to those of free space.) The lack of simultaneous occurrence of negative ε and μ in natural materials hindered further study on negative index materials (NIMs) for some 30 years. On the basis of theoretical work by Pendry et al. [9,10], Shelby et al. [11] first demonstrated that a metamaterial exhibits negative refraction at X-band microwave frequencies. In a NIM medium, the phase velocity of an electromagnetic (EM) wave is opposite to its energy flux. Light refracted from a conventional positive index material (PIM) into a NIM will bend to the same side of the surface normal as the incident beam (a phenomenon called negative refraction), and a flat slab of NIM can focus light [8]. Pendry [12] claimed that a NIM slab with $\varepsilon=\mu=-1$ performs the dual function of correcting the phase of the propagating components and amplifying the evanescent components, which normally exist only in the near field of the object. The combined effects could make a perfect lens that eliminates the limitations on image resolution imposed by diffraction for conventional lenses. Potential applications range from nanolithography to novel Bragg reflectors, phase-compensated cavity resonators, waveguides, and enhanced photon tunneling for microscale energy conversion devices [13–17]. Despite doubt cast by some researchers on the concept of a "perfect lens" and even on negative refraction, both hypotheses of negative refraction and the ability to focus light by a slab of NIM have been verified by analytical, numerical, and experimental methods [18–21].

A NIM layer of $\varepsilon=\mu=-1$, when placed together with a vacuum gap of the same thickness between two (semi-infinite) dielectric media, compensates the phase change in vacuum and causes evanescent wave amplification, so that radiative energy can be transmitted completely through the structure [16]. However, the ideal case of $\varepsilon=\mu=-1$ cannot exist at more than a single frequency because both ε and μ of a NIM must be inherently dependent on frequency [8]. Although some studies have dealt with nonideal cases [17,22], the effects of dispersion and loss on photon tunneling have not been completely understood. In the present study, the frequency-dependent complex ε and μ are considered, and enhanced photon tunneling is analyzed in terms of the excitation of a surface plasmon resonance. Furthermore, the effect of subdividing the NIM into thinner layers, which are placed alternately with vacuum gaps, is investigated to see whether structural changes can

[1]Corresponding author.

Contributed by the Heat Transfer Division for publication in the JOURNAL OF HEAT TRANSFER. Manuscript received: August 12, 2004. Final manuscript received: January 26, 2005. Review conducted by: Stefan Thynell.

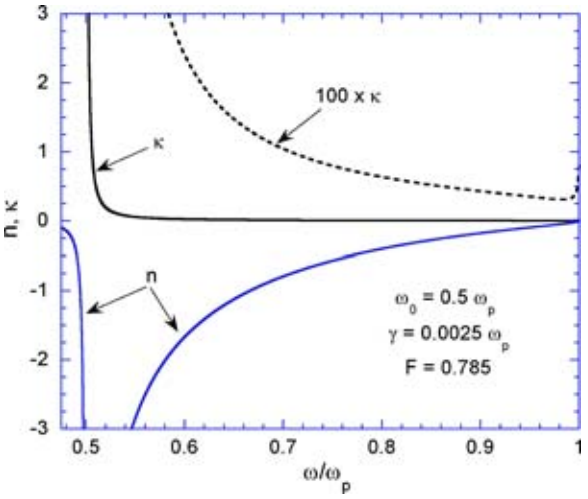

Fig. 1 Refractive index n and extinction coefficient κ of a NIM, calculated from Eqs. (1)–(3) as functions of the dimensionless frequency ω/ω_p. The dashed line shows the κ values multiplied by 100.

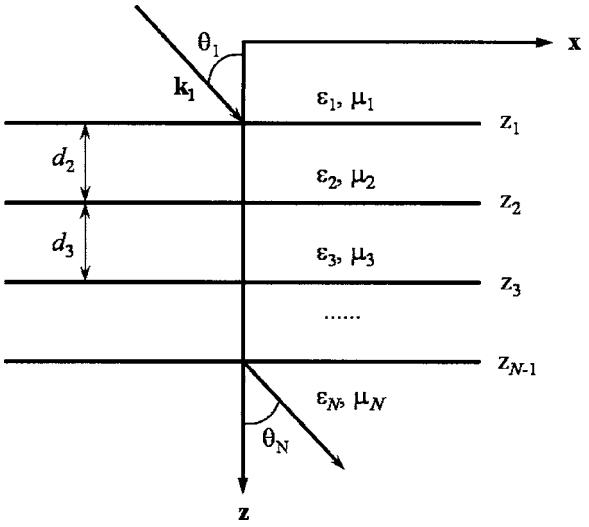

Fig. 2 Schematic illustration of a N-layer structure

significantly alter the radiative properties. Moreover, we provide a modified matrix formulation for use in the calculation.

2 Theory

Based on an effective medium approach, Pendry et al. [9,10] showed that the relative permittivity and permeability of the negative index metamaterial, consisting of repeated unit cells of interlocking copper strips and split-ring resonators, can be expressed as functions of the angular frequency ω as follows:

$$\varepsilon(\omega) = 1 - \frac{\omega_p^2}{\omega^2 + i\gamma_e\omega} \tag{1}$$

and

$$\mu(\omega) = 1 - \frac{F\omega^2}{\omega^2 - \omega_0^2 + i\gamma_m\omega} \tag{2}$$

where ω_p is the effective plasma frequency, ω_0 is the effective resonance frequency, γ_e and γ_m are the damping terms, and F is the fractional area of the unit cell occupied by the split ring. From Eqs. (1) and (2), both negative ε and μ can be realized in a frequency range between ω_0 and ω_p for an adequately small γ_e and γ_m. Here, the values of ω_0, ω_p, γ_e, γ_m, and F depend on the geometry of the unit cell that constructs the metamaterial. In the present study, the following parameters are chosen: $\omega_0=0.5\omega_p$, $F=0.785$, and $\gamma_e=\gamma_m=\gamma$ with γ allowed to vary from zero to a small fraction of ω_p. Because of the scaling capability of the metamaterial [23], the frequency is normalized to ω_p in all the calculated results. The complex refractive index of the metamaterial depends on both ε and μ; hence,

$$\tilde{n}^2(\omega) = [n(\omega) + i\kappa(\omega)]^2 = \varepsilon(\omega)\mu(\omega) \tag{3}$$

Although the refractive index $n(\omega)$ may be negative, the extinction coefficient $\kappa(\omega)$ must be non-negative for a passive medium. The calculated n and κ are plotted in Fig. 1 as functions of the dimensionless frequency ω/ω_p for $\gamma=0.0025\omega_p$. It can be seen that in the frequency range from ω_0 to ω_p, where the real parts of ε and μ are negative, n is negative and κ (for small values of γ) is small at frequencies not too close to ω_0.

The transfer matrix method is a standard and convenient technique for calculating the radiative properties of multilayer structures [24–27]. It is assumed that the incident light is in a plane-wave form. Some modifications are necessary for the matrix formulation to be applicable to absorbing media and with NIMs. Even in some recent publications involving NIMs [13,16,17,28,29], the equations were either not provided or given under restricted conditions. The multilayer structure containing N layers is shown in Fig. 2. Each layer is assumed isotropic and can be fully described by a relative permittivity ε_l and a relative permeability μ_l ($l=1,2,\ldots N$). The transmittance of this multilayer structure can be expressed as

$$T = \frac{\mathrm{Re}(k_{Nz}^*/\mu_N^*)}{\mathrm{Re}(k_{1z}^*/\mu_1^*)}\left|\frac{1}{M_{11}}\right|^2, \quad \text{for } s \text{ polarization} \tag{4}$$

and

$$T = \frac{\mathrm{Re}(k_{Nz}/\varepsilon_N)}{\mathrm{Re}(k_{1z}/\varepsilon_1)}\left|\frac{1}{M_{11}}\right|^2, \quad \text{for } p \text{ polarization} \tag{5}$$

Here, Re takes the real part of a complex number, the asterisk denotes the complex conjugate, k_{lz} is the normal component of the wave vector of the lth layer, and M_{11} is the element of the transfer matrix $\mathbf{M}$, which is given by

$$\mathbf{M} = \begin{pmatrix} M_{11} & M_{12} \\ M_{21} & M_{22} \end{pmatrix} = \prod_{l=1}^{N-1} \mathbf{P}_l \mathbf{D}_l^{-1} \mathbf{D}_{l+1} \tag{6}$$

where $\mathbf{D}_l^{-1}$ is the inverse matrix of $\mathbf{D}_l$, given by

$$\mathbf{D}_l = \begin{pmatrix} 1 & 1 \\ k_{lz}/\mu_l & -k_{lz}/\mu_l \end{pmatrix}, \quad \text{for } s \text{ polarization} \tag{7}$$

and

$$\mathbf{D}_l = \begin{pmatrix} 1 & 1 \\ k_{lz}/\varepsilon_l & -k_{lz}/\varepsilon_l \end{pmatrix}, \quad \text{for } p \text{ polarization} \tag{8}$$

and

$$\mathbf{P}_l = \begin{pmatrix} e^{-ik_{lz}d_l} & 0 \\ 0 & e^{ik_{lz}d_l} \end{pmatrix} \tag{9}$$

where d_l is the thickness of the lth layer except that d_1 is set to zero, and k_{lz} is calculated from

$$k_x^2 + k_{lz}^2 = \varepsilon_l\mu_l\omega^2/c^2 \tag{10}$$

where c is the speed of light in vacuum and k_x (the wave-vector component parallel to the surface) is the same in all layers as required by the phase-matching condition. Note that the imaginary part of k_{lz} calculated from Eq. (10) should not be less than zero. The reflectance of the multilayer structure for either polarization can be calculated by

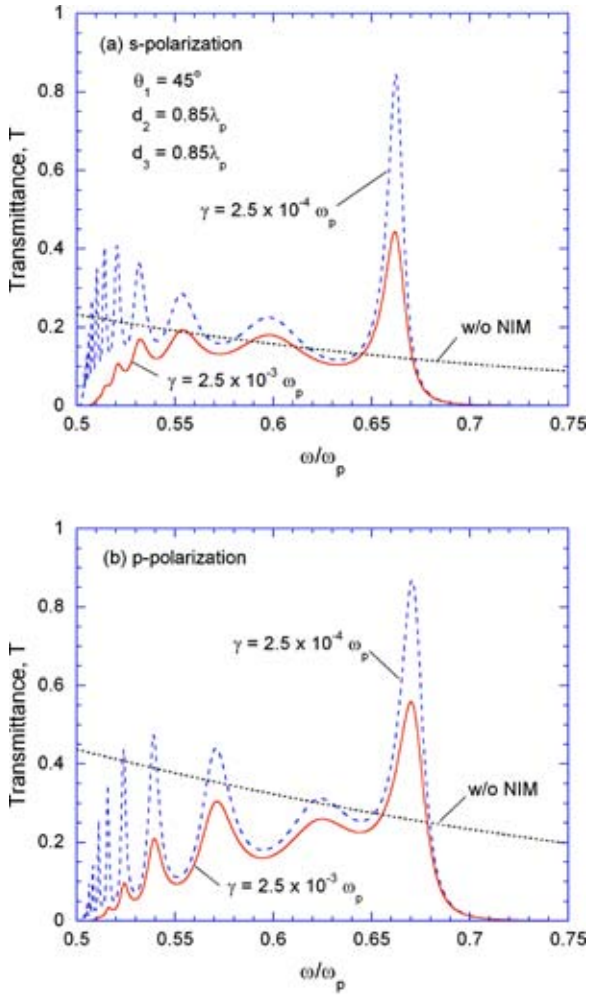

Fig. 3 Spectral transmittance of a four-layer structure at 45 deg incidence angle: (*a*) *s* polarization and (*b*) *p* polarization. For the dielectrics: $\varepsilon_1=\varepsilon_4=2.25$ and $\mu_1=\mu_4=1$; medium 2 is vacuum: $\varepsilon_2=\mu_2=1$; for the NIM: ε_3 and μ_3 are calculated from Eqs. (1) and (2) with $\omega_0/\omega_p=0.5$, $F=0.875$, and with different values of γ. The vacuum gap (VG) width and the NIM layer thickness are both taken to be $0.85\lambda_p$. The transmittance without a NIM layer ($d_3=0$) is also shown for comparison.

$$R=|M_{21}/M_{11}|^2 \tag{11}$$

It should be pointed out that the reflectance is ill defined when the first medium is dissipative because of the coupling between the reflected and incident waves [30]. However, Eqs. (4)–(11) are applicable if the last medium is dissipative.

3 Results and Discussion

Consider a four-layer ($N=4$) structure similar to that used in previous works [16,17]. The first and last media are semi-infinite dielectrics with $\varepsilon_1=\varepsilon_4=2.25$ ($n_1=n_4=1.5$). There are two intermediate layers: layer 2 is a vacuum gap (VG) and layer 3 is made of a NIM. In the present study, however, ε_3 and μ_3 are calculated from Eqs. (1) and (2). Without the NIM layer, the structure is similar to that used for the study of radiative transfer between two closely spaced plates [1,5]. For radiation from medium 1, the incidence angle should be greater than the critical angle $\theta_c=\arcsin(1/n_1)$ in order for photon tunneling to occur. This can be done by shaping the first dielectric like a prism, as in the attenuated total reflectance (ATR) configuration [31–33].

The calculated spectral transmittance at 45 deg angle of incidence is plotted in Fig. 3, for $\gamma=0.0025\omega_p$ and $0.00025\omega_p$, and compared to the case without the NIM layer ($d_3=0$). The VG width (d_2) and the NIM layer thickness (d_3) are both set to $0.85\lambda_p$, where $\lambda_p=2\pi c/\omega_p$ is the wavelength corresponding to the plasma frequency. The dimensionless approach allows the results to be scalable toward different electromagnetic spectral regions, once suitable negative index materials are available. For both polarizations, the transmittance oscillates in the frequency range from $0.5<\omega/\omega_p<0.7$, with a distinct peak between 0.65 and 0.68, and then goes to zero abruptly. The oscillation in the transmittance at $\omega/\omega_p<0.65$ is due to the interference of propagating waves inside the NIM layer, coupled with photon tunneling through the VG. On the other hand, the peak transmittance is due to the excitation of a surface plasma polariton (SPP) at the interface between the vacuum and NIM, to be discussed in the following.

A SPP is a coupled, localized electromagnetic wave that propagates along the interface of two different media and decay exponentially away from the interface [31]. In other words, there exists an evanescent wave in each medium whose amplitude is maximal at the interface. The excitation frequency of SPP depends not only on the electromagnetic properties of the materials but also on the wave-vector component k_x. At the interface between layer 2 (vacuum) and layer 3 (NIM) of the four-layer structure, the SPP dispersion relations satisfy the following simple equations when the thicknesses d_2 and d_3 extend to infinity and the loss (dissipation) in the NIM is negligible [32]:

$$\frac{\beta_2}{\mu_2}+\frac{\beta_3}{\mu_3}=0, \quad \text{for } s \text{ polarization} \tag{12}$$

and

$$\frac{\beta_2}{\varepsilon_2}+\frac{\beta_3}{\varepsilon_3}=0, \quad \text{for } p \text{ polarization} \tag{13}$$

where β_l is positive and is related to the wave vector by $\beta_l=(k_x^2-\varepsilon_l\mu_l\omega^2/c^2)^{1/2}$, $l=2$ or 3. Based on Eq. (10), for β to be positive, k_{lz} must be purely imaginary and evanescent waves occur in both media. Another necessary criterion for surface polariton to exist is that $\mu_3<0$ for s polarization and $\varepsilon_3<0$ for p polarization. The simultaneous negative ε and μ in a NIM allow SPPs to be excited for both polarizations in the same frequency region. Note that $k_x=(\omega n_1/c)\sin\theta_1$, Eqs. (12) and (13) can be recast as follows:

$$\sin\theta_1=\frac{1}{n_1}\left(\frac{\mu_3^2-\mu_3\varepsilon_3}{\mu_3^2-1}\right)^{1/2}, \quad \text{for } s \text{ polarization} \tag{14}$$

and

$$\sin\theta_1=\frac{1}{n_1}\left(\frac{\varepsilon_3^2-\varepsilon_3\mu_3}{\varepsilon_3^2-1}\right)^{1/2}, \quad \text{for } p \text{ polarization} \tag{15}$$

For a given angle of incidence θ_1 from a dielectric medium (layer 1), the frequency at which SPP can be excited, ω_{spp}, is the solution of Eq. (14) or (15) for each polarization. Generally speaking, θ_1 must be sufficiently large such that k_z is purely imaginary in both media 2 and 3. For the four-layer structure with finite thicknesses and nonzero γ, ω_{SPP} from Eq. (14) or (15) gives an approximate value to the excitation frequency of SPPs at the second interface. The excitation of polaritons causes a resonance transfer of the photon energy to a surface electromagnetic wave and is manifested in an ATR configuration as a sharp decrease in the reflectance [31]. In the case when a propagating wave exists in the last medium (layer 4), however, the excitation of SPPs can enhance the energy transmission via photon tunneling [33].

Table 1 compares ω_{SPP} calculated from Eqs. (14) and (15) at different incidence angles with the frequency ($\omega_{\max}$) that corresponds to the transmittance peak shown in Fig. 3 for $\gamma=0.0025\omega_p$. The agreement is very good, especially at larger incidence angles. The small deviation at θ_1 close to the critical angle θ_c (41.8 deg in this case) is caused by the disturbance of end layers. As can be seen from Fig. 3, $\omega_{\max}$ changes little with γ but

Table 1 Comparison of the SPP frequency ω_{spp} calculated from Eqs. (14) and (15) to the frequency ω_{max} corresponding to the transmittance peak for the four-layer structure with $\gamma = 0.0025\omega_p$.

Incidence angle (deg)	*s* polarization		*p* polarization	
	ω_{spp}/ω_p	ω_{max}/ω_p	ω_{spp}/ω_p	ω_{max}/ω_p
42	0.66600	0.66350	0.66650	0.66550
45	0.66325	0.66175	0.67075	0.67025
50	0.65975	0.65925	0.67625	0.67625
55	0.65750	0.65725	0.68025	0.68050
60	0.65550	0.65550	0.68325	0.68350

the magnitude of transmittance decreases significantly when γ is increased. The sharp peaks of transmittance due to SPP excitations suggest a possible way to build new optical resonators, similar to the Fabry-Perot resonators [26,34], which have important applications in optoelectronics and optical communications.

Because both d_2 and d_3 are finite, the matching of thickness is critical for transmittance enhancement [17]. In the lossless case, $\beta_2 d_2 = \beta_3 d_3$ is referred to as a phase-matching condition [16] because it will result in a transmittance of unity. When loss is included, the optimization condition can no longer be expressed by a simple relation. The peak transmittance of the four-layer structure as a function of d_3 is shown in Fig. 4 for different γ values, where the VG width d_2 is fixed to $0.85\lambda_p$. The frequency corresponding to the transmittance peak shifts slightly from the values (ω_{max}) listed in Table 1 as d_3 changes. The value of d_3 that results in a maximal transmittance depends on polarization because the SPP resonance frequencies are different. For a given γ, there exists an optimum d_3 at which the peak transmittance is the highest. Using $d_3 = d_2\beta_2/\beta_3$ and under the lossless assumption, one obtains $d_3 = 1.02\lambda_p$ for *s* polarization and $0.7\lambda_p$ for *p* polarization, close to optimum values for $\gamma = 0.00025\omega_p$ as shown in Fig. 4. As γ is increased to $0.0025\omega_p$, the optimum d_3 is reduced especially for *s* polarization.

Polaritons can be excited at both surfaces of a NIM slab [35]. If the media on both sides of the slab are identical, the two surface polaritons are coupled. On the other hand, a standing wave may exist inside a slab while the outside fields decay exponentially. Such a mode is called a waveguide mode or a bulk polariton [31]. Both coupled and bulk polaritons may affect the radiative properties [33]. Assume that a five-layer structure is constructed by equally subdividing the vacuum gap into two layers that sandwich the NIM layer. The two end layers are the same dielectric media as in the four-layer structure. The thickness of the NIM layer remains to be $0.85\lambda_p$, which is equal to the total thickness of the vacuum gaps. The results for both *s* and *p* polarizations are plotted in Fig. 5(*a*) for $\theta_1 = 45$ deg and Fig. 5(*b*) for $\theta_1 = 60$ deg. Compared to Fig. 3, the transmittance in Fig. 5(*a*) near the SPP frequency has increased remarkably. Furthermore, the full width at half maximum of the peak is significantly broadened. In particular, the peak at the SPP frequency for *s* polarization splits into two peaks. This change of the transmittance spectrum is because of the coupling between the SPPs at both surfaces of the NIM layer [31,35]. The split of the SPP mode depends on the field coupling strength. It follows that the split SPP modes tend to be more separated for a thinner NIM layer, whereas they shift to each other for a thicker NIM layer and eventually the fields inside the NIM decouple and the split SPP modes restore when the NIM thickness approaches infinity. The broadening of the transmittance peak shown in Fig. 5(*a*) is because the two split SPP modes are very close to each other, especially for *p* polarization, such that the corresponding two peaks overlap. The field reinforcement inside the NIM due to the coupling gives rise to the large enhancement of the tunneling transmittance, and this enhancement is more remarkable at larger incidence angles, such as the case shown in Fig. 5(*b*), where the transmittance near the SPP frequency is over 20 times greater than that without a NIM layer.

An alternative way to construct a five-layer structure is to place the vacuum gap in the middle and equally subdivide the NIM into two layers located between the VG and a dielectric. The transmittance of this five-layer structure is shown in Figs. 5(*c*) and 5(*d*) for an incidence angle equal to 45 and 60 deg, respectively. The label NIM/VG/NIM indicates that the vacuum gap is between two subdivided NIM layers. In the calculation, the VG thickness and the total NIM thickness remain to be $0.85\lambda_p$. The transmittance features due to SPP excitation are similar to those seen in Figs. 5(*a*) and 5(*b*), except that discernable split of the peak is for *p* polarization instead of *s* polarization. For $\omega/\omega_p < 0.6$, the transmittance shown in Figs. 5(*c*) and 5(*d*) is lower and less oscillating as compared to the corresponding results in Figs. 5(*a*) and 5(*b*). The reason for this difference is that the transmittance is enhanced in the case with VG/NIM/VG by the excitation of the waveguide modes or bulk polaritons inside the NIM layer. A slab should have a larger refractive index (absolute value) than its surrounding media in order to sustain bulk polaritons; this is the case for Figs. 5(*a*) and 5(*b*). Consequently, there are no bulk polaritons in Figs. 5(*c*) and 5(*d*). A detailed discussion of the dispersion relations of

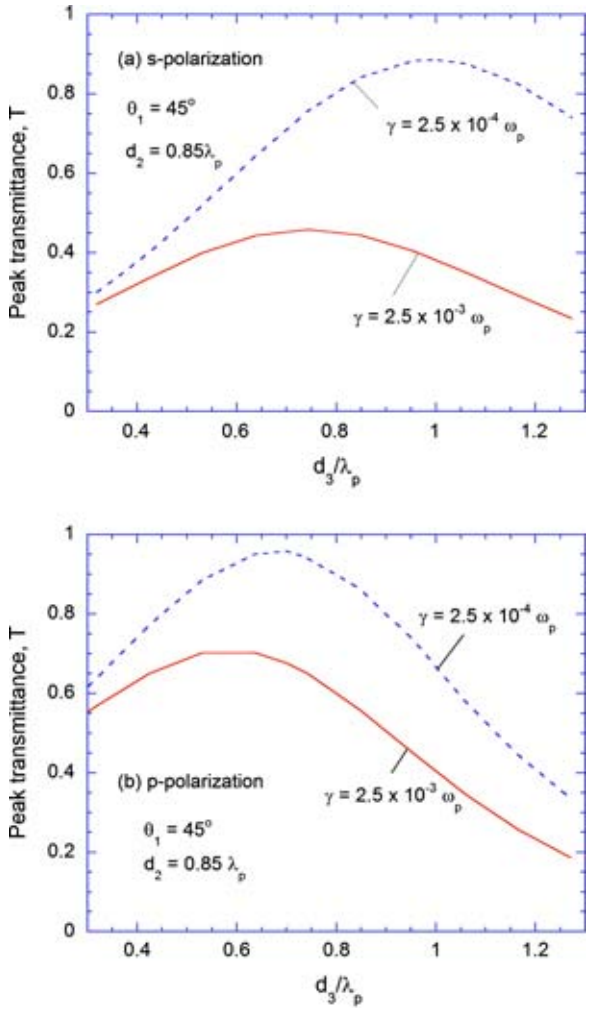

Fig. 4 Peak transmittance of the four-layer structure versus the thickness of the NIM for incidence angle of 45 deg, when d_2 is fixed at $0.85\lambda_p$: (*a*) *s* polarization and (*b*) *p* polarization.

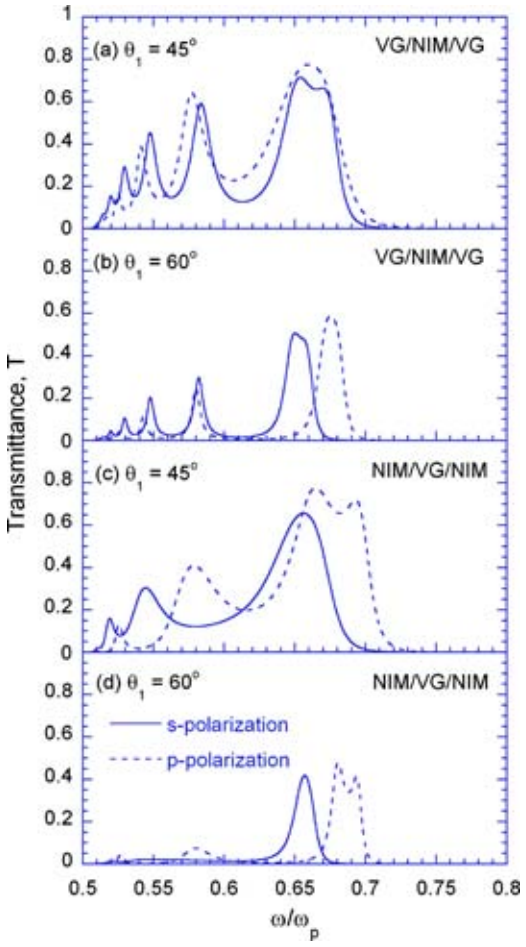

Fig. 5 The transmittance spectra of a five-layer structure for $\gamma=0.0025\omega_p$. In (*a*) and (*b*), the VG is equally divided into two layers sandwiching the NIM layer. The total thickness of the VGs and the thickness of the NIM layer are the same as in Fig. 4, i.e., $0.85\lambda_p$. In (*c*) and (*d*), the NIM layer is equally divided into two layers that sandwich the VG.

bulk polaritons can be found in the work of Park et al. [33]. The transmittance peaks for $\omega/\omega_p<0.6$ in Figs. 5(*a*) and 5(*b*) correspond to the modes of bulk polaritons excited in the NIM slab. Bulk polaritons have important applications in integrated optical waveguides [36] and for inducing resonant tunneling superlattices [37]. Figure 5 demonstrates that a NIM slab, which sustains bulk polaritons, can enhance radiative energy transmission via photon tunneling.

The focusing capability of a NIM slab may be the most promising application of these metamaterials. Challenges remain to reduce the losses in practical devices. It was shown [28,29] that the image resolution could be improved by dividing the NIM slab used in the imaging device into many thinner lamellae, and it was thought that the subdivision would result in a reduced absorption in the NIM. Many thinner NIM layers, when placed alternately with vacuum gaps, can cause stronger field coupling inside the structure when SPPs are excited. Therefore better enhancement of photon tunneling may be achieved. For instance, a six-layer structure can be made by equally dividing each VG and NIM layer into two sublayers and placing them alternately between the two end dielectrics. A ten-layer structure can be constructed by doubling the number of VGs and NIM layers without increasing the total thicknesses. The transmittance of multilayer structures calculated using the matrix formulation is shown in Figs. 6(*a*) for *s* polarization and 6(*b*) for *p* polarization, at 60 deg incidence angle. Clearly, the transmittance increases after each division and the frequency range over which significant tunneling can be observed is greatly broadened by subdividing the layers. The subdividing process results in more bulk polaritons or SPPs being excited and coupling inside the structure. The dispersion relations of bulk and surface modes are very complicated when the structure consists of many layers. Nevertheless, when the layers between the two end dielectrics become thinner and thinner, the stronger SPP coupling will split the surface modes into many branches: some modes will shift to higher frequencies and thus broaden the frequency range, whereas some others will shift to lower frequencies and can convert to bulk polaritons [33].

In order to understand the radiative properties for both propagating modes and evanescent modes, the transmittance and absorptance at a single frequency $\omega=0.665\omega_p$ is plotted in Figs. 7(*a*) for *s* polarization and 7(*b*) for *p* polarization, as a function of the incidence angle. When the incidence angle is smaller than the critical angle (at the dielectric-air interface), the radiative properties are affected by multiple reflections and interferences of the propagating waves in the layered structure. Consequently, a decrease in transmittance is observed when the layer number is increased from 4 to 10, presumably because of the enhancement of reflectance as more boundaries are added. On the other hand, when the incidence angle is greater than the critical angle, bulk polaritons and surface polaritons may be excited and may interact with each other to enhance the electromagnetic field in the structure, resulting in an enhancement in the transmittance as the num-

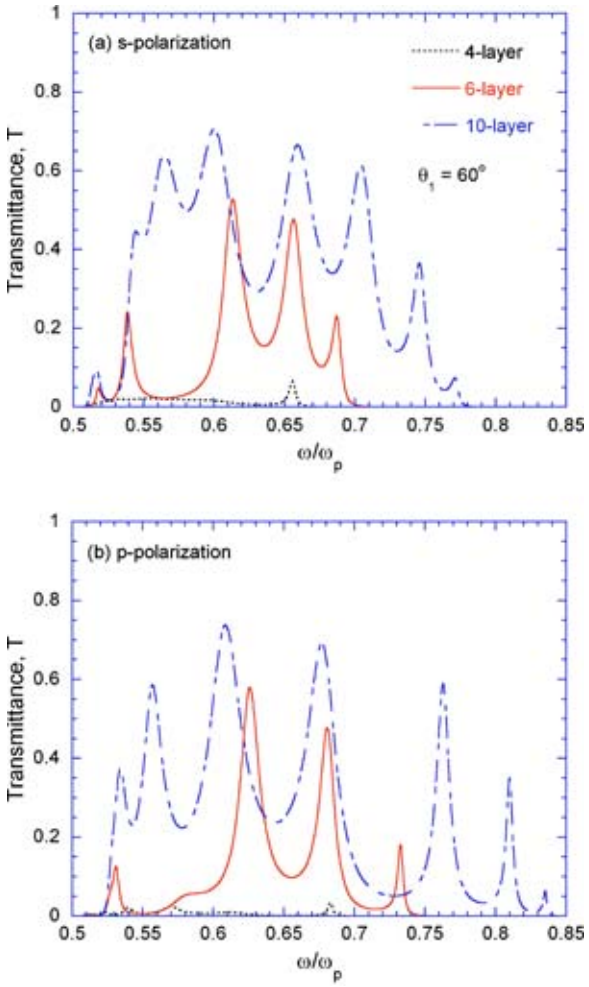

Fig. 6 The transmittance spectra of multilayer structures with different numbers of layers at an incidence angle θ_1=60 deg: (*a*) *s* polarization and (*b*) *p* polarization. Parameters for calculating $\varepsilon(\omega)$ and $\mu(\omega)$ of the NIM are the same as those used for Fig. 5. In each multilayer structure a VG and a NIM layer of the same thickness are alternately placed between the two end layers. The total thickness of the VGs is the same as the total thickness of the NIM layers and is set to $0.85\lambda_p$, the same as in Figs. 3 and 5.

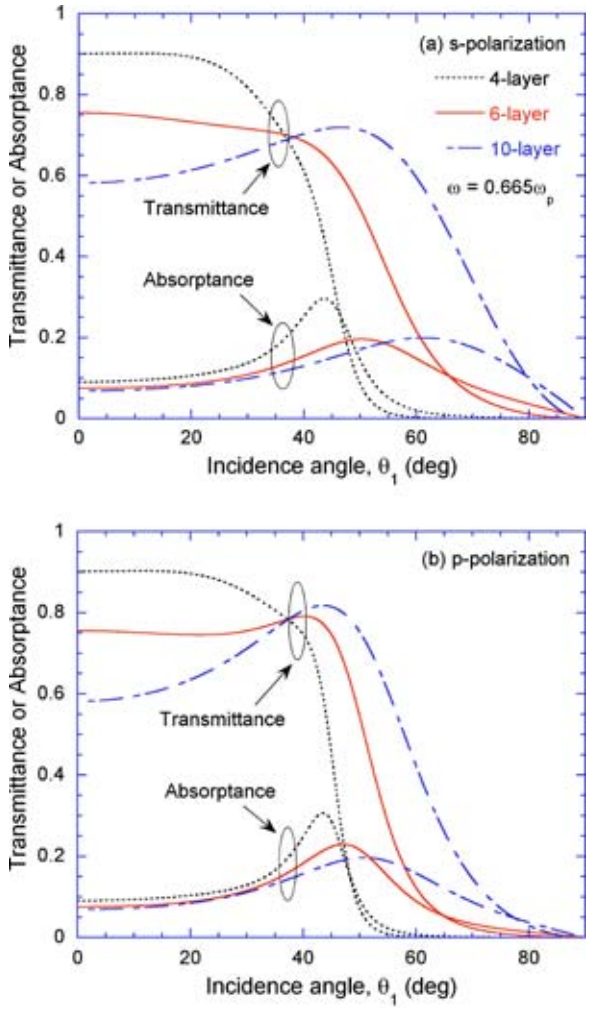

Fig. 7 The transmittance and absorptance of multilayer structures, with different number of layers, versus the incidence angle θ_1. (*a*) *s* polarization and (*b*) *p* polarization. The configurations are the same as corresponding ones in Fig. 6 and the frequency is fixed at ω=0.665ω_p.

ber of layers is increased. Increasing the magnitude of evanescent waves at the image plane is key to the improved image quality using NIM multilayer structures [28,29]. Contrary to intuition, however, the enhancement in transmission is not necessarily due to a reduction of absorption by subdivision of the NIM layers. It can be seen from Fig. 7 that the absorptance increases with the number of layers at large incidence angles. Hence, the enhanced transmission of evanescent waves is associated with a reduction of reflection.

4 Conclusions

The phenomenon of photon tunneling by using NIM layers in a multilayer structure is investigated. Enhanced energy transmission via photon tunneling is found when surface or bulk polaritons are excited. The enhancement depends on the thickness of the NIM layer that should be tuned to satisfy the phase matching condition between VG and NIM layer. Furthermore, it is found that subdividing the NIM layers into many thinner layers and placing them alternately with VGs can greatly enhance energy transmission, especially at large incidence angles. The enhancement is attributed to the coupling of surface or bulk polaritons that reinforce the EM fields in the structure. By coupling more photons into the structure, a large increase in the transmission of evanescent waves and a reduction of the reflectance are observed using multilayer structures. Devices that depend on photon tunneling to transfer energy or optical signals have wide applications in microscale energy conversion and optical communication. The result of the present study may benefit future applications of NIMs.

Acknowledgment

This work was supported by the National Science Foundation through Grants No. CTS-0082969, No. CTS-0236831, and No. CTS-0327117. Thanks to Keunhan Park and Bong Jae Lee for helpful comments.

Nomenclature

c = speed of light in vacuum, 2.998×10^8 m/s
d = layer thickness, m
F = fractional area of the unit cell occupied by the split ring
i = $\sqrt{-1}$
k_x = wave-vector component in the x direction, 1/m
k_z = wave-vector component in the z direction, 1/m
$\mathbf{M}$ = transfer matrix

n = real part of $\tilde{n}$
$\tilde{n}$ = complex refractive index
R = reflectance
T = transmittance

Greek Symbols

β = evanescent wave-decaying factor, 1/m
γ = damping term, rad/s
ε = relative (electric) permittivity
θ_1 = angle of incidence
κ = imaginary part of $\tilde{n}$
λ_p = wavelength corresponding to the plasma frequency, m
μ = relative (magnetic) permeability
ω = angular frequency, rad/s
ω_0 = resonance frequency, rad/s
ω_p = plasma frequency, rad/s
ω_{spp} = surface plasmon polariton resonance frequency, rad/s

References

[1] Cravalho, E. G., Tien, C. L., and Caren, R. P., 1967, "Effect of Small Spacing on Radiative Transfer Between Two Dielectrics," ASME J. Heat Transfer, **89**, pp. 351–358.
[2] Tien, C. L., and Cunnington, G. R., 1973, "Cryogenic Insulation Heat Transfer," Adv. Heat Transfer, **9**, pp. 349–417.
[3] Reddick, R. C., Warmack, R. J., and Ferrell, T. J., 1989, "New Form of Scanning Optical Microcopy," Phys. Rev. B, **39**, pp. 767–770.
[4] Kawata, S., 2001, "Near-Field Microscope Probes Utilizing Surface Plasmon Polaritons," in *Near-Field Optics and Surface Plasmon Polaritons*, S. Kawata, ed., Springer-Verlag, Berlin, pp. 15–27.
[5] Whale, M. D., and Cravalho, E. G., 2002, "Modeling and Performance of Microscale Thermophotovoltaic Energy Conversion Devices," IEEE Trans. Energy Convers., **17**, pp. 130–142.
[6] Mulet, J. P., Joulain, K., Carminati, R., and Greffet, J.-J., 2002, "Enhanced Radiative Heat Transfer at Nanometric Distance," Microscale Thermophys. Eng., **6**, pp. 209–222.
[7] Narayanaswamy, A., and Chen, G., 2003, "Surface Modes for Near Field Thermophotovoltaics," Appl. Phys. Lett., **82**, pp. 3544–3546.
[8] Veselago, V. G., 1968, "The Electrodynamics of Substances With Simultaneously Negative Values of ε and μ," Sov. Phys. Usp., **10**, pp. 509–514.
[9] Pendry, J. B., Holden, A. J., Stewart, W. J., and Youngs, I., 1996, "Extremely Low Frequency Plasmons in Metallic Mesostructures," Phys. Rev. Lett., **76**, pp. 4773–4776.
[10] Pendry, J. B., Holden, A. J., Rubbins, D. J., and Stewart, W. J., 1999, "Magnetism from Conductors and Enhanced Nonlinear Phenomena," IEEE Trans. Microwave Theory Tech., **47**, pp. 2075–2084.
[11] Shelby, R. A., Smith, D. R., and Schultz, S., 2001, "Experimental Verification of a Negative Index of Refraction," Science, **292**, pp. 77–79.
[12] Pendry, J. B., 2000, "Negative Refraction Makes a Perfect Lens," Phys. Rev. Lett., **85**, pp. 3966–3969.
[13] Gerardin, J., and Lakhtakia, A., 2002, "Negative Index of Refraction and Distributed Bragg Reflections," Microwave Opt. Technol. Lett., **34**, pp. 409–411.
[14] Engheta, N., 2002, "An Idea for Thin Subwavelength Cavity Resonators Using Metamaterials With Negative Permittivity and Permeability," IEEE Antennas Wireless Propag. Lett., **1**, pp. 10–13.
[15] Qing, D.-K., and Chen, G., 2004, "Enhancement of Evanescent Waves in Waveguides Using Metamaterials of Negative Permittivity and Permeability," Appl. Phys. Lett., **84**, pp. 669–671.
[16] Zhang, Z. M., and Fu, C. J., 2002, "Unusual Photon Tunneling in the Presence of a Layer With a Negative Refractive Index," Appl. Phys. Lett., **80**, pp. 1097–1099.
[17] Fu, C. J., and Zhang, Z. M., 2003, "Transmission Enhancement Using a Negative-Refraction Layer," Microscale Thermophys. Eng., **7**, pp. 221–234.
[18] Zhang, Z. M., and Park, K., 2004, "On the Group Front and Group Velocity in a Dispersive Medium Upon Refraction From a Nondispersive Medium," J. Heat Transfer, **126**, pp. 244–249.
[19] Foteinopoulou, S., Economou, E. N., and Soukoulis, C. M., 2003, "Refraction in Media With a Negative Refractive Index," Phys. Rev. Lett., **90**, pp. 107402/1–4.
[20] Parazzoli, C. G., Greegor, R. B., Li, K., Koltenbah, B. E. C., and Tanielian, M., 2003, "Experimental Verification and Simulation of Negative Index of Refraction Using Snell's Law," Phys. Rev. Lett., **90**, pp. 107401/1–4.
[21] Houck, A. A., Brock, J. B., and Chuang, I. L., 2003, "Experimental Observations of a Left-Handed Material That Obeys Snell's Law," Phys. Rev. Lett., **90**, pp. 137401/1–4.
[22] Smith, D. R., Schurig, D., Rosenbluth, M., Schultz, S., Ramakrishna, S. A., and Pendry, J. B., 2003, "Limitations on Subdiffraction Imaging With a Negative Refractive Index Slab," Appl. Phys. Lett., **82**, pp. 1506–1508.
[23] Yen, T. J., Padilla, W. J., Fang, N., Vier, D. C., Smith, D. R., Pendry, J. B., Basov, D. N., and Zhang, X., 2004, "Terahertz Magnetic Response From Artificial Materials," Science, **303**, pp. 1494–1496.
[24] Born, M., and Wolf, E., 1999, *Principles of Optics*, 7th Edition, Cambridge University Press, Cambridge, UK, pp. 54–74.
[25] Kong, J. A., 1990, *Electromagnetic Wave Theory*, 2nd Edition, Wiley, New York, pp. 126–138.
[26] Yeh, P., 1988, *Optical Waves in Layered Media*, Wiley, New York, pp. 102–113.
[27] Zhang, Z. M., Fu, C. J., and Zhu, Q. Z., 2003, "Optical and Thermal Radiative Properties of Semiconductors Related to Micro/Nanotechnology," Adv. Heat Transfer, **37**, pp. 179–296.
[28] Ramakrishna, S. A., Pendry, J. B., Wiltshire, M. C. K., and Stewart, W. J., 2003, "Imaging the Near Field," J. Mod. Opt., **50**, pp. 1419–1430.
[29] Gao, L., and Tang, C. J., 2004, "Near-Field Imaging by a Multilayer Structure Consisting of Alternate Right-Handed and Left-Handed Materials," Phys. Lett. A, **322**, pp. 390–395.
[30] Zhang, Z. M., 1997, "Reexamination of the Transmittance Formulae of a Lamina," J. Heat Transfer, **119**, pp. 645–647.
[31] Raether, H., 1988, *Surface Plasmons on Smooth and Rough Surfaces and on Gratings*, Springer-Verlag, Berlin, Chap. 2.
[32] Ruppin, R., 2000, "Surface Polaritons of a Left-Handed Medium," Phys. Lett. A, **277**, pp. 61–64.
[33] Park, K., Lee, B. J., Fu, C. J., and Zhang, Z. M., 2005, "Study of the Surface and Bulk Polaritons With a Negative Index Metamaterial," J. Opt. Soc. Am. B, **22**, pp. 1016–1023.
[34] Kumar, A. R., Boychev, V. A., Zhang, Z. M., and Tanner, D. B., 2000, "Fabry-Perot Resonators Built With $YBa_2Cu_3O_{7-\delta}$ Films on Si Substrates," ASME J. Heat Transfer, **122**, pp. 785–791.
[35] Ruppin, R., 2001, "Surface Polaritons of a Left-Handed Material Slab," J. Phys.: Condens. Matter, **13**, pp. 1811–1819.
[36] Buckman, B., 1992, *Guided Wave Photonics*, Sauders College Publishing, New York, pp. 35–85.
[37] Yeh, P., 1985, "Resonant Tunneling of Electromagnetic Radiation in Superlattice Structures," J. Opt. Soc. Am. A, **2**, pp. 568–571.